Naunyn-Schmiedeberg's Archives of Pharmacology
https://doi.org/10.1007/s00210-026-05747-2

RESEARCH

Induction of differential cytotoxicity and ROS-driven severe genomic DNA damage and intrinsic mitochondrial apoptosis by erbium oxide nanoparticles in *p53*-compromised human NSCLC cells

Hanan R. H. Mohamed[1] · Alaa H. Elsewedy[2] · Shahd Mosaad[2] · Aya A. Osman[2] · Habiba M. Zaki[2] · Mayada E. Borai[2] · Ayman Diab[2] · Gehan Safwat[2]

Received: 10 June 2026 / Accepted: 16 July 2026

Abstract

Non-small cell lung cancer (NSCLC) remains a leading cause of cancer-related mortality worldwide, with current therapeutic strategies limited by systemic toxicity, drug resistance, and poor tumor selectivity. These limitations highlight the urgent need for safer, targeted therapeutic strategies. In this context, erbium oxide nanoparticles (Er_2O_3NPs) have attracted attention in biomedical research due to their unique physicochemical characteristics, yet their potential as anticancer agents against NSCLC remains fully unexplored. This study was consequently conducted to assess the anticancer efficacy and underlying mechanisms of Er_2O_3NPs in human A549 NSCLC cells, alongside with evaluating their safety in normal WI-38 lung fibroblasts. Cytotoxicity was determined using the MTT assay, and genomic DNA integrity was assessed via the alkaline Comet assay. Oxidative stress and mitochondrial function were evaluated through 2′,7′-dichlorodihydrofluorescein diacetate (2,7-DCFH-DA) and Rhodamine-123 staining, respectively. Apoptotic induction was analyzed using DAPI nuclear staining and chromatin diffusion assays, while qRT-PCR quantified the expression of apoptosis- and mitochondria-related genes. Er_2O_3NPs exhibited concentration-dependent cytotoxicity in A549 cells (IC_{50} = 93.46 µg/ml) and lower toxicity in WI-38 fibroblasts (IC_{50} = 147.5 µg/ml), yielding a selectivity index of 1.58. Mechanistically, treating A549 cells at the IC_{50} concentration for 72 h induced severe genomic DNA damage, excessive ROS generation, and pronounced mitochondrial membrane depolarization. DAPI staining revealed characteristic apoptotic nuclear changes, including chromatin condensation and fragmentation, while the chromatin diffusion assay demonstrated extensive DNA dispersion indicative of advanced apoptotic DNA degradation. Moreover, qRT-PCR analysis showed significant downregulation of *p53*, *Bcl-2*, and *ND3* gene expression. Given the inherent mutant *p53* status of A549 cells, this transcriptional downregulation indicates that Er_2O_3NPs bypass canonical wild-type *p53* transcriptional activation, triggering instead an ROS-driven intrinsic mitochondrial apoptotic signaling pathway. In conclusion, Er_2O_3NPs induce preferential cytotoxicity in NSCLC cells through ROS-mediated severe genomic DNA damage and intrinsic mitochondrial dysfunction within a *p53*-compromised genetic background. These findings suggest that Er_2O_3NPs hold potential as a nanotherapeutic candidate for NSCLC. However, further in vivo studies, targeted delivery systems, and direct protein-level evaluations are warranted to fully clarify these mechanisms and advance their clinical applicability.

Keywords Erbium oxide nanoparticles · Non-small cell lung cancer · A549 cells · Reactive oxygen species · Genomic DNA damage · Mitochondrial apoptosis

Introduction

Lung cancer remains the foremost cause of cancer-related mortality worldwide, surpassing breast, colorectal, and prostate cancers combined. Its high incidence, aggressive progression, and poor survival rates make it a critical global health challenge. Among its subtypes, non-small cell lung cancer (NSCLC) accounts for approximately 85% of all

✉ Hanan R. H. Mohamed
hananesresm@yahoo.com; hananeeyra@cu.edu.eg

[1] Department of Zoology, Faculty of Science, Cairo University, Giza, Egypt

[2] Faculty of Biotechnology, October University for Modern Sciences and Arts (MSA), 6th of October City, Egypt

Published online: 23 July 2026

cases, making it the most prevalent and clinically significant form of the disease (Sung et al. 2021; Bray et al. 2024; Siegel et al. 2025). Despite advances in diagnostic imaging, molecular profiling, and therapeutic strategies, the global incidence of NSCLC continues to rise, largely driven by persistent exposure to major risk factors, including tobacco smoking, the strongest contributor, as well as air pollution, occupational carcinogens such as asbestos and radon, and inherited genetic predispositions (Travis et al. 2015; Herbst et al. 2018). NSCLC poses a particular threat due to its aggressive biological behavior. The disease often develops silently and remains asymptomatic in its early stages, which delays detection in most patients. Consequently, the majority of cases are diagnosed at advanced or metastatic stages, when curative options are limited (Nasim et al. 2019).

Even with multimodal treatment approaches, NSCLC is characterized by high recurrence rates and rapid metastatic progression, complicating management and worsening clinical outcomes. The overall prognosis for patients with advanced NSCLC remains poor, with five-year survival rates below 25% despite ongoing improvements in therapeutic strategies (Herbst et al. 2018). Current therapeutic options for NSCLC include surgery, radiotherapy, targeted therapy, immunotherapy, and chemotherapy. Chemotherapy, while remains a mainstay, its clinical utility is severely constrained by systemic toxicity, poor tumor selectivity, multidrug resistance, and limited long-term efficacy (Duma et al. 2019; 2022). Chemotherapeutic agents frequently induce adverse effects such as nephrotoxicity, myelosuppression, hepatotoxicity, and neuropathy, which compromise both treatment outcomes and patient quality of life (Sung et al. 2021; Duma et al. 2019). These limitations underscore the urgent need for novel therapeutic strategies capable of selectively eradicating malignant cells while sparing normal lung tissue.

Nanotechnology-based therapies have recently emerged as promising alternatives due to their ability to improve drug delivery, enhance tumor targeting, and minimize systemic toxicity (Patra et al. 2018; Chehelgerdi et al. 2023). Among these, rare-earth metal oxide nanoparticles have attracted considerable attention for their unique physicochemical, redox, and optical properties (Mehtab et al. 2022; Safwat et al. 2022). Erbium oxide nanoparticles (Er_2O_3NPs), in particular, are biocompatible and capable of generating reactive oxygen species (ROS) under physiological conditions, making them potential candidates for inducing selective cytotoxicity in cancer cells (Safwat et al. 2022; Mohamed et al. 2025). Emerging evidences indicate that Er_2O_3NPs trigger oxidative stress, mitochondrial dysfunction, and apoptosis in malignant cell lines: Hep-G2 hepatocellular carcinoma and U937 lymphoma cells (Safwat et al. 2022; Mohamed et al. 2025), Nevertheless, their therapeutic potential in lung cancer, particularly NSCLC, remains fully unexplored. Although earlier reports demonstrated cytotoxic and pro-apoptotic effects of Er_2O_3NPs in models such as hepatocellular carcinoma, and lymphoma, these findings cannot be directly extrapolated to NSCLC because each cancer type exhibits distinct molecular signatures, redox status, metabolic demands, and nanoparticle-uptake characteristics. NSCLC cells, particularly A549, have unique antioxidant defenses, mitochondrial dynamics, and resistance pathways that may modulate their responsiveness to nanoparticle-induced oxidative stress and apoptosis. Therefore, dedicated evaluation in NSCLC is essential to determine whether Er_2O_3NPs exert comparable, diminished, or even distinct mechanistic effects in lung cancer cells.

Given the rising global incidence of NSCLC, the high mortality rates associated with advanced disease, and the shortcomings of conventional chemotherapy, there is a pressing need to investigate the therapeutic potential of Er_2O_3NPs as novel anticancer agents. Accordingly, this study was designed to explore the cytotoxic, genotoxic, and apoptotic effects of Er_2O_3NPs in A549 NSCLC cells, with parallel assessment of their safety in normal human WI-38 lung fibroblasts. By examining genomic stability, ROS generation, mitochondrial membrane potential, and apoptosis-related gene expression, this work aims to provide new mechanistic insights into the anticancer activity of Er_2O_3NPs and their potential role as targeted nanotherapeutics for NSCLC.

Materials and methods

Chemicals

Er_2O_3NPs were obtained from Sigma-Aldrich (St. Louis, MO, USA) as a faint pink powder with an average particle size of < 100 nm and a purity of 99.9% trace metals basis. The nanoparticles were cataloged under CAS No. 12061–16-4, EC No. 235–045-7, and Product No. 203238. All additional chemicals and reagents used throughout the study were of molecular biology grade. Dimethyl sulfoxide (DMSO), 3-(4,5-dimethylthiazol-2-yl)−2,5-diphenyl tetrazolium bromide (MTT), ethidium bromide, low- and normal-melting-point agarose, Tris base, ethylenediaminetetraacetic acid (EDTA), Rhodamine-123, 4′,6-diamidino-2-phenylindole (DAPI), 2′,7′-dichlorodihydrofluorescein diacetate (DCFH-DA), trypan blue, and other routine laboratory reagents were purchased from Sigma-Aldrich (St. Louis, MO, USA). Cell culture reagents, including Dulbecco's Modified Eagle Medium (DMEM), HEPES buffer, L-glutamine, gentamicin, and trypsin–EDTA, were obtained from Lonza (Verviers, Belgium). The culture medium was supplemented with 10% fetal bovine serum (FBS), and phenol red-free DMEM was used for assays requiring spectrophotometric

or fluorescence measurements to minimize background interference. All reagents were freshly prepared according to the manufacturers' instructions, and all experimental procedures were performed under aseptic conditions in a Class II biological safety cabinet to ensure sterility and experimental reproducibility.

Characterization of Er_2O_3NPs

The Er_2O_3NPs used in this study were chemically synthesized and had been previously characterized in detail by Mohamed and colleagues (Safwat et al. 2022; Mohamed et al. 2025). Briefly, the physicochemical properties of Er_2O_3NPs were evaluated using X-ray diffraction (XRD) to determine phase composition and crystallinity, transmission electron microscopy (TEM) to examine particle morphology and primary particle size, and dynamic light scattering (DLS) coupled with zeta potential analysis to determine the hydrodynamic particle size distribution and surface charge in aqueous suspension. XRD analysis confirmed the high purity and crystallographic integrity of the synthesized Er_2O_3NPs, with diffraction peaks consistent with standard reference data for crystalline erbium oxide, indicating the formation of cubic Er_2O_3NPs. DLS measurements revealed a bimodal hydrodynamic size distribution, with approximately 89.3% of the suspended nanoparticles exhibiting an average diameter of 570.7 nm and 10.7% displaying an average diameter of 95.35 nm, reflecting particle aggregation in suspension. Consistently, the zeta potential was low, indicating limited colloidal stability. In contrast, TEM analysis of ultrasonicated samples demonstrated well-dispersed Er_2O_3NPs with predominantly cubic morphology and primary particle sizes of approximately 50–60 nm (Safwat et al. 2022; Mohamed et al. 2025). Therefore, prior each experiment, Er_2O_3NPs suspensions were ultrasonicated for 30 min to minimize aggregation and ensure homogeneous nanoparticle dispersion prior to cellular exposure.

Ethical considerations

This study did not involve human participants, human subjects, or the collection or use of primary human tissues. All experiments were performed exclusively using established human cancer cell lines that were commercially purchased from accredited cell repositories. The cell lines were handled, cultured, and maintained in strict accordance with the suppliers' instructions and relevant institutional and international laboratory guidelines and regulations. As no direct experimentation on humans or human-derived tissue samples was conducted, institutional ethical approval was not required for this work.

Culture and maintenance of normal WI and cancerous A549 cells

Normal human WI-38 lung fibroblasts and A549 human non-small cell lung carcinoma cells were obtained from the Regional Center for Mycology and Biotechnology, Al-Azhar University (Cairo, Egypt). Each cell line was cultured separately in high-glucose DMEM (4.5 g/L) supplemented with 10% heat-inactivated FBS, gentamicin (50 µg/ml), penicillin (100 U/ml), and streptomycin (100 U/ml). Cells were incubated at 37 °C in a humidified atmosphere containing 5% CO_2, and the culture medium was renewed every 2–3 days. Cells were subcultured using 0.25% trypsin–EDTA upon reaching 70–80% confluence. All experiments were performed using low-passage A549 and WI-38 cells (passages 5–15) to minimize passage-related phenotypic variation and ensure experimental reproducibility. Only healthy, exponentially growing cultures with $\geq 90\%$ viability were used for all experiments. Cell morphology and confluence were routinely monitored throughout the study to ensure optimal culture conditions. Preliminary optimization experiments also confirmed adequate baseline metabolic activity in both cell lines, validating their suitability for MTT-based cytotoxicity assessment and ensuring that changes in MTT reduction reflected the effects of Er_2O_3NP treatment rather than inherent metabolic differences between the two cell lines.

Estimation of Er_2O_3NPs cytotoxicity in normal WI and cancerous A549 lung cells

The cytotoxic potential of Er_2O_3NPs on normal human lung fibroblasts (WI-38) and human non-small cell lung carcinoma cells (A549) was determined using the MTT colorimetric assay, following previously described procedures with minor modifications (Mosmann 1983; El-Zahabi et al. 2019; Abdelsalam et al. 2022). Briefly, WI-38 and A549 cells were independently seeded into sterile 96-well flat-bottom culture plates (Falcon, NJ, USA) at a density of 1×10^4 cells per well in 100 µl of complete DMEM medium. The culture medium was supplemented with 10% heat-inactivated FBS, 1% L-glutamine, 100 U/ml penicillin, and 100 µg/ml streptomycin. Cells were allowed to adhere for 24 h at 37 °C in a humidified incubator containing 5% CO_2. After the attachment period, the culture medium was carefully removed and replaced with fresh DMEM containing two-fold serial concentrations of Er_2O_3NPs (7.80, 15.60, 31.25, 62.50, 125.00, 250.00, 500.00, and 1000.00 µg/ml). Each treatment concentration was evaluated in triplicate wells, whereas untreated control cells received nanoparticle-free culture medium. Cells were then incubated with Er_2O_3NPs for 72 h.

Following the exposure period, the treatment medium was aspirated and substituted with 100 µl of phenol red-free DMEM, after which 10 µl of MTT reagent (12 mM; 5 mg/ml

in PBS) was added to each well. The plates were incubated for 4 h at 37 °C in the dark, allowing metabolically active cells to reduce MTT into insoluble purple formazan crystals. To dissolve the crystals, 85 µl of the medium was removed, and 50 µl of dimethyl sulfoxide (DMSO) was added to each well. The plates were then incubated for an additional 10 min at 37 °C to ensure complete solubilization. The absorbance of the resulting solution was recorded at 590 nm using a microplate reader (SunRise, TECAN, USA). Cell viability was calculated according to the following equation: Cell viability (%) = $(OD_T/OD_C) \times 100$; where OD_T represents the average absorbance of treated wells and OD_C corresponds to the mean absorbance of the untreated control wells. The half-maximal inhibitory concentration (IC_{50}) values were determined by nonlinear regression analysis using GraphPad Prism software (San Diego, CA, USA) based on data obtained from three independent experiments. To evaluate the preferential cytotoxicity toward cancer cells, the Selectivity Index (SI) was calculated as: SI = IC_{50} (WI-38)/IC_{50} (A549). An SI value greater than 1 indicates selective toxicity toward cancer cells. All results were expressed as mean ± standard deviation (SD).

Culture and treatment of cancerous A549 lung cancer cells

Human A549 non-small cell lung carcinoma cells were cultured in T25 tissue culture flasks containing DMEM medium supplemented with 10% heat-inactivated FBS, 1% L-glutamine, 100 U/ml penicillin, and 100 µg/ml streptomycin, following previously reported cell culture procedures (Mosmann 1983; El-Zahabi et al. 2019; Abdelsalam et al. 2022). The cultures were maintained at 37 °C in a humidified incubator with 5% CO_2 and allowed to proliferate until they reached approximately 70–80% confluence. For experimental evaluation, A549 cells were randomly divided into two groups. The vehicle untreated control group received complete culture medium containing ≤ 0.1% dimethyl sulfoxide (DMSO), corresponding to the final solvent concentration used for Er_2O_3NPs preparation, to exclude any potential effects of the vehicle itself. This concentration of DMSO is widely regarded as non-cytotoxic under standard cell culture conditions. The treated group was exposed to Er_2O_3NPs at the IC_{50} concentration determined by the MTT assay in the present study. Both groups were incubated under identical culture conditions for 72 h before subsequent analyses (El-Zahabi et al. 2019; Abdelsalam et al. 2022).

After the treatment period, cells were harvested using 0.25% trypsin–EDTA, followed by centrifugation at 1500 rpm for 5 min at 4 °C. The resulting cell pellets were washed twice with ice-cold phosphate-buffered saline (PBS, pH 7.4) to remove residual culture medium and nanoparticle traces. Finally, the pellets were resuspended in PBS and stored at − 80 °C until further biochemical and molecular analyses were performed (El-Zahabi et al. 2019; Abdelsalam et al. 2022). All experiments were conducted in triplicate to ensure reproducibility and statistical reliability. Furthermore, all experimental procedures were carried out under aseptic laboratory conditions and in accordance with established institutional and international guidelines for good laboratory practice.

Estimation of Er_2O_3NPs-induced genomic instability in A549 lung cancer cells

Genomic instability in non-small A549 lung carcinoma cells following exposure to the IC_{50} concentration of Er_2O_3NPs for 72 h was assessed using the alkaline comet assay, as described by Tice et al. (2000) and Langie et al. (2015). A suspension of ~ 10,000 cells in 15 µL PBS was mixed with 60 µl of 0.5% low-melting-point agarose (37 °C) and immediately spread onto microscope slides pre-coated with 1% normal-melting-point agarose. After solidification for 30 min at room temperature, slides were immersed in cold lysis buffer (2.5 M NaCl, 100 mM EDTA, 10 mM Tris–HCl, pH 10) containing 1% Triton X-100 and 10% DMSO, and incubated for 24 h at 4 °C in the dark. Slides were then placed in alkaline electrophoresis buffer (300 mM NaOH, 1 mM EDTA, pH 12) for 15 min to allow DNA unwinding, followed by electrophoresis at 25 V, 300 mA for 30 min at 4 °C. After electrophoresis, slides were neutralized with 0.4 M Tris–HCl buffer (pH 7.5) for 5 min, fixed in cold ethanol for 5 min, and air-dried. Staining was performed with 50 µL ethidium bromide (20 µg/mL), and samples were examined under a fluorescence microscope. For each treatment, 50 randomly selected nuclei per slide were analyzed using COMETSCORE™ software. DNA damage was quantified using tail length, % DNA in tail, and tail moment. Data are expressed as mean ± SD from three independent experiments, with statistical analysis performed to assess the genotoxic effects of Er_2O_3NPs treatment in A549 lung cancer cells.

Evaluation of ROS generation within A549 lung cancer cells

Intracellular ROS production in non-small A549 lung carcinoma cells after 72 h exposure to the IC_{50} concentration of Er_2O_3NPs was quantified using the fluorescent probe 2′,7′-dichlorofluorescin diacetate (2,7-DCFH-DA), following the method of Siddiqui et al. (2010). Briefly, equal volumes of the A549 cell suspension and 20 µM 2,7-DCFH-DA solution were mixed in sterile microcentrifuge tubes and incubated in the dark at room temperature for 30 min. Inside the cells, the probe was enzymatically deacetylated to form non-fluorescent DCFH, which was then oxidized by ROS to

the highly fluorescent compound 2′,7′-dichlorofluorescein (DCF). After staining, cells were gently spread onto clean glass slides to form a thin monolayer and examined under an epifluorescence microscope equipped with DCF-compatible filters. Images were captured at 200 × magnification from randomly selected fields using identical exposure settings. Fluorescence intensity, representing intracellular ROS levels, was quantified using *Fiji* (ImageJ) software. Relative fluorescence values of treated and untreated control cells were compared to determine the extent of ROS generation. All experiments were conducted in triplicate to ensure reproducibility and statistical reliability.

Monitoring mitochondrial integrity in A549 lung cancer cells

Mitochondrial membrane potential, a critical marker of mitochondrial integrity and early apoptosis, was evaluated in non-small A549 lung carcinoma cells after 72 h exposure to Er_2O_3NPs at the IC_{50} concentration. The assay was performed using Rhodamine-123, a cationic, cell-permeable fluorescent dye that selectively accumulates in polarized mitochondria, following the protocol of Zhang et al. (2011). Briefly, equal volumes of the cell suspension and Rhodamine-123 working solution (10 µg/ml) were mixed in sterile, light-protected microcentrifuge tubes and incubated at 37 °C for 1 h in the dark to allow dye uptake by active mitochondria. After incubation, cells were washed twice with cold PBS to remove unbound dye, then mounted on pre-cleaned, labeled glass slides and covered with sterile coverslips. Slides were examined under an epifluorescence microscope equipped with Rhodamine-123 filters, and images were captured at 200 × magnification from randomly selected fields using identical exposure settings. Fluorescence intensity, reflecting mitochondrial polarization, was quantified using *Fiji* (ImageJ) software. A significant reduction in Rhodamine-123 fluorescence in treated cells compared with untreated control cells indicated mitochondrial depolarization, a hallmark of early mitochondrial dysfunction and apoptosis. All experiments were performed in triplicate, and results were expressed as mean ± SD to ensure reproducibility and statistical significance.

Assessment of apoptosis induction in A549 lung cancer cells

Apoptosis, a programmed cell death, is a vital mechanism for maintaining cellular homeostasis and eliminating damaged or malignant cells. Inducing apoptosis is a major therapeutic strategy in cancer management, and its detection is essential for evaluating the efficacy of anticancer agents. In this study, apoptosis induction in non-small A549 lung carcinoma cells after exposure to Er_2O_3NPs at the IC_{50} concentration was assessed using two complementary approaches: the chromatin diffusion assay, which detects DNA fragmentation linked to apoptotic signaling, and 4′,6-diamidino-2-phenylindole (DAPI) nuclear staining, which visualizes characteristic apoptotic features such as chromatin condensation and nuclear fragmentation.

Chromatin diffusion assay

The chromatin diffusion assay detects apoptotic DNA fragmentation by exploiting alkali-labile DNA sites that, under alkaline conditions, produce diffusion halos within an agarose matrix (Singh 2000). Microscope slides were pre-coated with 0.7% normal-melting-point agarose, then A549 cells were suspended in low-melting-point agarose and layered onto the coated slides. After air drying, slides were immersed in cold lysis buffer for 10 min to remove cytoplasmic contents while preserving nuclear DNA. Slides were then neutralized with Tris buffer, fixed in cold ethanol, and stained with ethidium bromide. Apoptotic cells were identified under a fluorescence microscope by the presence of characteristic DNA halos. For each sample, 1,000 cells were analyzed, and the percentage of apoptotic cells was calculated. All assays were performed in triplicate to ensure reproducibility.

DAPI nuclear staining

To confirm apoptosis induction in Er_2O_3NPs-treated A549 lung cancer cells, nuclear morphology was screened using DAPI, a DNA-binding fluorescent dye that highlights apoptotic features such as chromatin condensation and nuclear fragmentation (Guan and Guan 2020). A549 cells were seeded into 96-well plates at a density of 1×10^4 cells/well and treated with Er_2O_3NPs at the IC50 concentration for 72 h. After treatment, cells were washed with PBS, fixed in 4% paraformaldehyde, and stained with DAPI (1 µg/ml) for 1 h in the dark. Stained cells were washed and examined under a fluorescence microscope at 200 × magnification using a DAPI filter. Apoptotic cells were identified by condensed or fragmented nuclei and apoptotic body formation, while non-apoptotic cells showed uniform nuclear staining. For each group, 1,000 cells were counted, and the apoptotic index was calculated. All experiments were performed in triplicate, and data were expressed as mean ± SD.

Profiling of *p53*, *ND3* and *Bcl2* gene expression in A549 lung cancer cells

To further evaluate the effects of Er_2O_3NPs on mitochondrial function and apoptosis, the expression of pro-apoptotic *p53*, mitochondrial *ND3* (a key component of the electron transport chain), and anti-apoptotic *Bcl2* genes was quantified in

A549 lung cancer cells following 72 h treatment with the IC_{50} concentration of Er_2O_3NPs. Total RNA was extracted from treated and untreated control A549 cells using the GeneJET RNA Purification Kit (Thermo Fisher Scientific, USA) according to the manufacturer's instructions. RNA purity and concentration were verified with a NanoDrop spectrophotometer. From each sample, 1 µg RNA was reverse transcribed into cDNA using the High-Capacity cDNA Reverse Transcription Kit (Applied Biosystems, USA). Quantitative real-time PCR (qRT-PCR) was then performed using SYBR Green PCR Master Mix ((Sigma-Aldrich St. Louis, MO, USA)) and gene-specific primers shown in Table 1 on a StepOnePlus Real-Time PCR System (Applied Biosystems), following optimized cycling conditions (Suzuki et al. 1999; Lai et al. 2013; Grzybowska-Szatkowska and Ślaska 2014). GAPDH served as the internal reference gene. Relative gene expression levels of *p53, ND3*, and *Bcl2* were calculated using the ΔΔCt method. All reactions were run in triplicate, and data were expressed as mean ± SD from three independent experiments.

Table 1 Sequences of primers used in qRT-PCR

Gene	Strand	Primer's sequences
GAPDH	Forward	5'-GAAGGTGAAGGTCGGAGTCA-3'
	Reverse	5'-GAAGATGGTGATGGGATTTC-3'
ND3	Forward	5'-CGCCGCCTGATACTGGCAT-3'
	Reverse	5'-CTAGTATTCCTAGAAGTGAG-3'
BCL-2	Forward	5'-TCCGATCAGGAAGGCTAGAGT-3'
	Reverse	5'-TCGGTCTCCTAAAAGCAGGC-3'
P53	Forward	5'-CAGCCAAGTCTGTGACTTGCACGTAC-3'
	Reverse	5'-CTATGTCGAAAAGTGTTTCTGTCATC-3'

This analysis provided mechanistic insights into how Er_2O_3NPs regulate apoptotic signaling and mitochondrial function in A549 cells.

Statistical analysis

All results are expressed as mean ± SD and analyzed using Statistical Package for the Social Sciences (SPSS) software. Statistical differences in DNA damage, gene expression, apoptotic cell counts, and other measured parameters between Er_2O_3NPs-treated and untreated control A549 cells were assessed using an unpaired two-tailed Student's t-test. A p-value < 0.05 was considered statistically significant.

Results

Er_2O_3NPs induce selective cytotoxicity in malignant A549 lung cells versus normal WI-38 lung fibroblasts

MTT assay results demonstrated a clear, concentration-dependent reduction in the viability of non-small A549 lung cancer cells following 72 h of exposure to serial two-fold dilutions of Er_2O_3NPs (7.80, 15.60, 31.25, 62.50, 125.00, 250.00, 500.00, and 1000.00 µg/ml), as shown in Fig. 1. The IC_{50} value for A549 cells was found equal to 93.46 µg/ml; confirming the potent cytotoxic activity of Er_2O_3NPs against malignant A549 lung cells. In contrast, normal WI-38 lung fibroblasts exhibited markedly higher resistance, with an IC_{50} of 147.50 µg/ml under identical treatment conditions. This discrepancy yielded a selectivity index (SI) of 1.58, indicating preferential cytotoxicity toward cancerous A549 lung cancer cells while sparing normal WI fibroblasts. These findings highlight the therapeutic potential of Er_2O_3NPs as

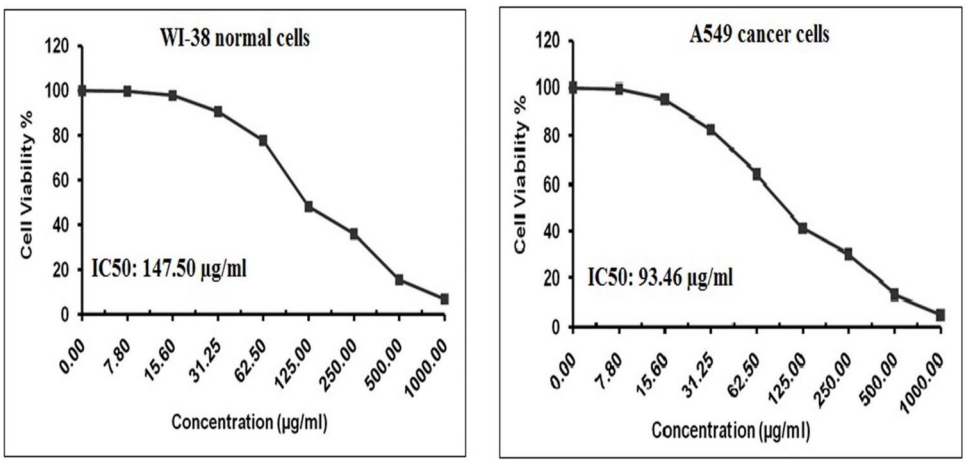

Fig. 1 Viability of human non-small A549 lung cancer cells assessed using the MTT assay exposure to Er_2O_3NPs at two-fold increasing concentrations (7.8, 15.6, 31.25, 62.5, 125, 250, 500 and 1000 µg/ml) for 72 h

targeted nanotherapeutics for lung cancer and justify further mechanistic studies at the IC_{50} concentration to elucidate their anticancer mode of action.

Er_2O_3NPs induce genomic instability in A549 lung cancer cells

Interpretation of the alkaline comet results demonstrated that exposure of non-small A549 lung cancer cells to Er_2O_3NPs at the IC_{50} concentration (93.46 µg/ml) for 72 h resulted in marked genomic DNA damage. This genotoxic effect was evidenced by the highly significant increases in tail length ($p < 0.001$), %DNA in tail ($p < 0.01$), and tail moment ($p < 0.001$) compared with untreated control A549 cells, as displayed in Table 2. These parameters are well-recognized indicators of DNA strand breaks and fragmentation, confirming the strong genotoxic activity of Er_2O_3NPs. Microscopic evaluation further supported these results: as depicted in Fig. 2 untreated cells displayed compact nuclei with minimal DNA migration, while Er_2O_3NPs-treated A549 cells exhibited distinct comet tails, characteristic of severe DNA fragmentation. Collectively, both quantitative and visual data clearly demonstrate that Er_2O_3NPs induce profound genomic instability in A549 lung cancer cells.

Er_2O_3NPs cause marked ROS overproduction in A549 lung cancer cells

As displayed in Fig. 3, exposure of non-small A549 lung cancer cells to Er_2O_3NPs at the IC_{50} concentration (93.46 µg/ml) for 72 h caused a significant elevation in the generation level of intracellular ROS. This was quantitatively demonstrated by a highly significant increase ($p < 0.001$) in the fluorescence intensity of 2′,7′-DCFH-DA, a ROS-sensitive fluorescent probe that fluoresces upon oxidation. Compared with untreated control cells, Er_2O_3NPs -treated A549 cells displayed markedly stronger fluorescence signals, confirming extensive ROS accumulation within the cytoplasm (Fig. 3). These findings indicate that Er_2O_3NPs trigger oxidative stress in A549 lung cancer cells and suggest that excessive ROS generation plays a central role in their cytotoxic mechanism.

Er_2O_3NPs induce severe mitochondrial dysfunction in A549 lung cancer cells

Assessment of mitochondrial membrane potential using Rhodamine-123, a cationic fluorescent dye that selectively accumulates in active mitochondria, revealed a pronounced loss of mitochondrial polarization in A549 lung

Table 2 Genomic DNA damage in human non-small A549 lung cancer following exposure to the IC50 concentration (93.46 µg/ml) of Er_2O_3NPs for 72 h

Cells	Treatment (Concentration)	Tail length (px)	%DNA in tail	Tail moment
A549 lung cancer cells	Untreated (0.00 µg/ml)	4.61 ± 0.23	18.35 ± 2.34	0.85 ± 0.21
	Er_2O_3NPs-treated (93.46 µg/ml)	19.73 ± 0.81 ***	30.28 ± 2.15 **	6.05 ± 0.21 ***

Results are expressed as mean ± SD

** and ***: Indicates statistical significant difference from the compared untreated control cells at $p < 0.01$ and $p < 0.001$, respectively, using *independent student t-test*

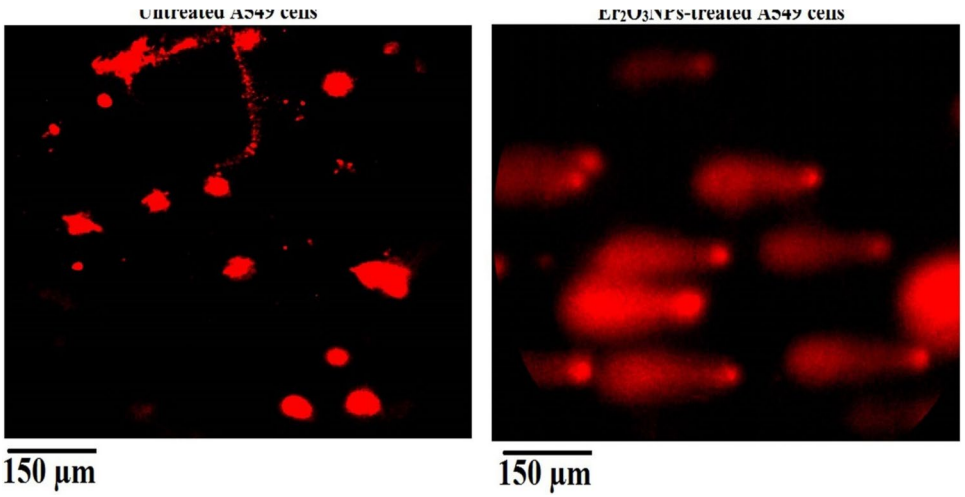

Fig. 2 Representative examples for the scored Comet nuclei with intact DNA in untreated A549 lung cancer cells and those with damaged DNA in A549 lung cancer cells treated with the IC50 concentration of Er_2O_3NPs (93.46 µg/ml) for 72 h. Magnification 200x

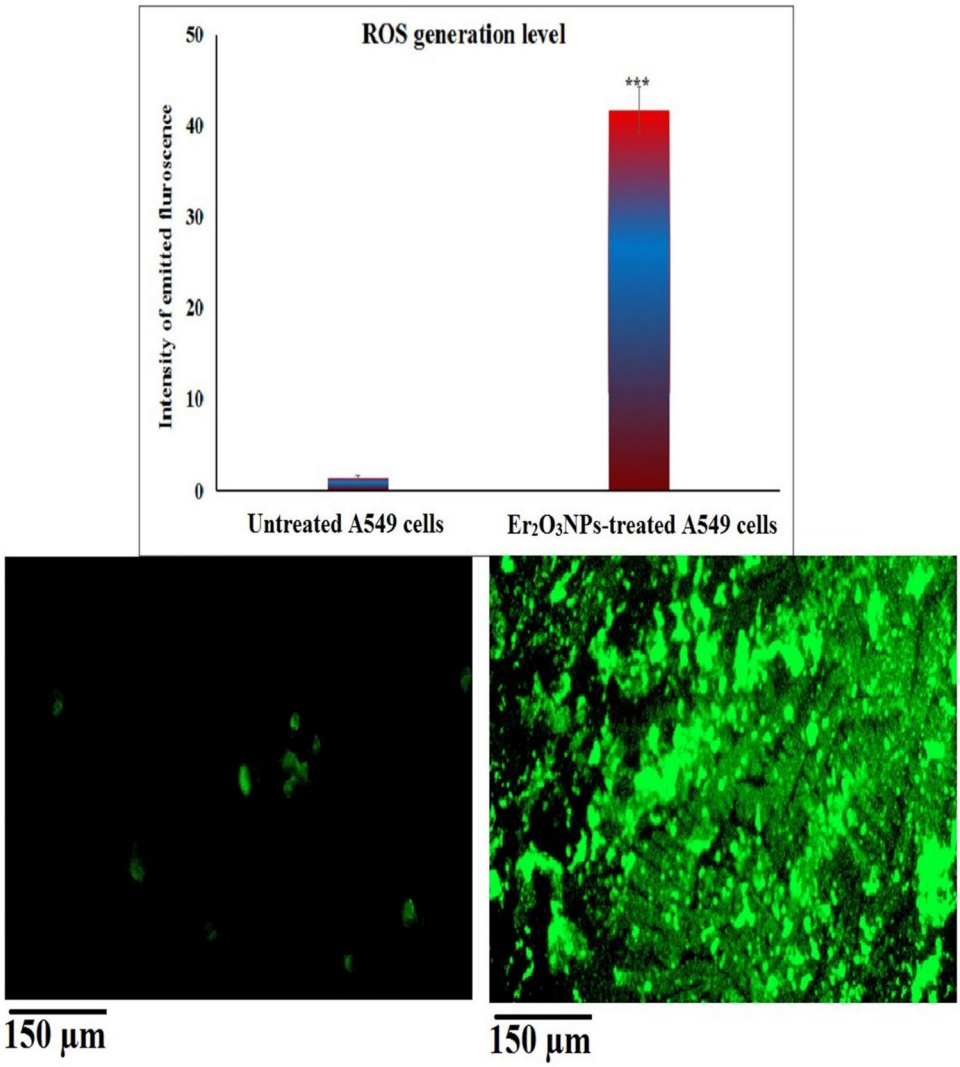

Fig. 3 Qualitative and quantitative estimation of ROS generation using 2′,7′-DCFH-DA dye within the untreated and treated non-small A549 lung cancer cells with the IC50 concentration (93.46 µg/ml) of Er_2O_3NPs for 72 h. Magnification 200x

cancer cells following 72 h of exposure to Er_2O_3NPs at the IC_{50} concentration (93.46 µg/ml). As shown in Fig. 4, this mitochondrial disruption was evidenced by a highly significant reduction ($p < 0.001$) in Rhodamine-123 fluorescence intensity in Er_2O_3NPs-treated cells compared to untreated control A549 cells. The observed marked decrease in fluorescence indicates mitochondrial membrane depolarization, reflecting a severe impairment of mitochondrial function and integrity induced by Er_2O_3NPs in A549 lung cancer cells. These findings suggest that mitochondrial dysfunction constitutes a major event in the Er_2O_3NPs-mediated cytotoxic pathway in non-small A549 lung cancer cells.

Er_2O_3NPs induce pronounced apoptotic cell death in A549 lung cancer cells

Apoptosis induction in non-small A549 lung cancer cells was confirmed after 72 h of exposure to Er_2O_3NPs at the IC_{50} concentration (93.46 µg/ml) using chromatin diffusion and DAPI nuclear staining assays. The combined results of these assays demonstrated significant apoptotic activity of Er_2O_3NPs, as evidenced by characteristic nuclear morphological alterations and extensive chromatin fragmentation. In the chromatin diffusion assay, Er_2O_3NPs-treated A549 cells displayed characteristic chromatin diffusion halos, indicative of apoptotic DNA fragmentation and dispersion into the cytoplasm. In contrast, untreated control A549 cells exhibited compact, intact nuclei with minimal diffusion (Fig. 5). Quantitative assessment demonstrated a highly significant increase ($p < 0.001$) in both the number and percentage of apoptotic Er_2O_3NPs-treated cells exhibiting DNA halos compared to untreated control A549 cells as reported in Table 3.

Complementary DAPI nuclear staining further validated these findings. Untreated control A549 cells displayed uniformly stained, smooth, and rounded nuclei, indicative of healthy normal morphology. In contrast, Er_2O_3NPs-treated A549 lung cancer cells exhibited hallmark apoptotic

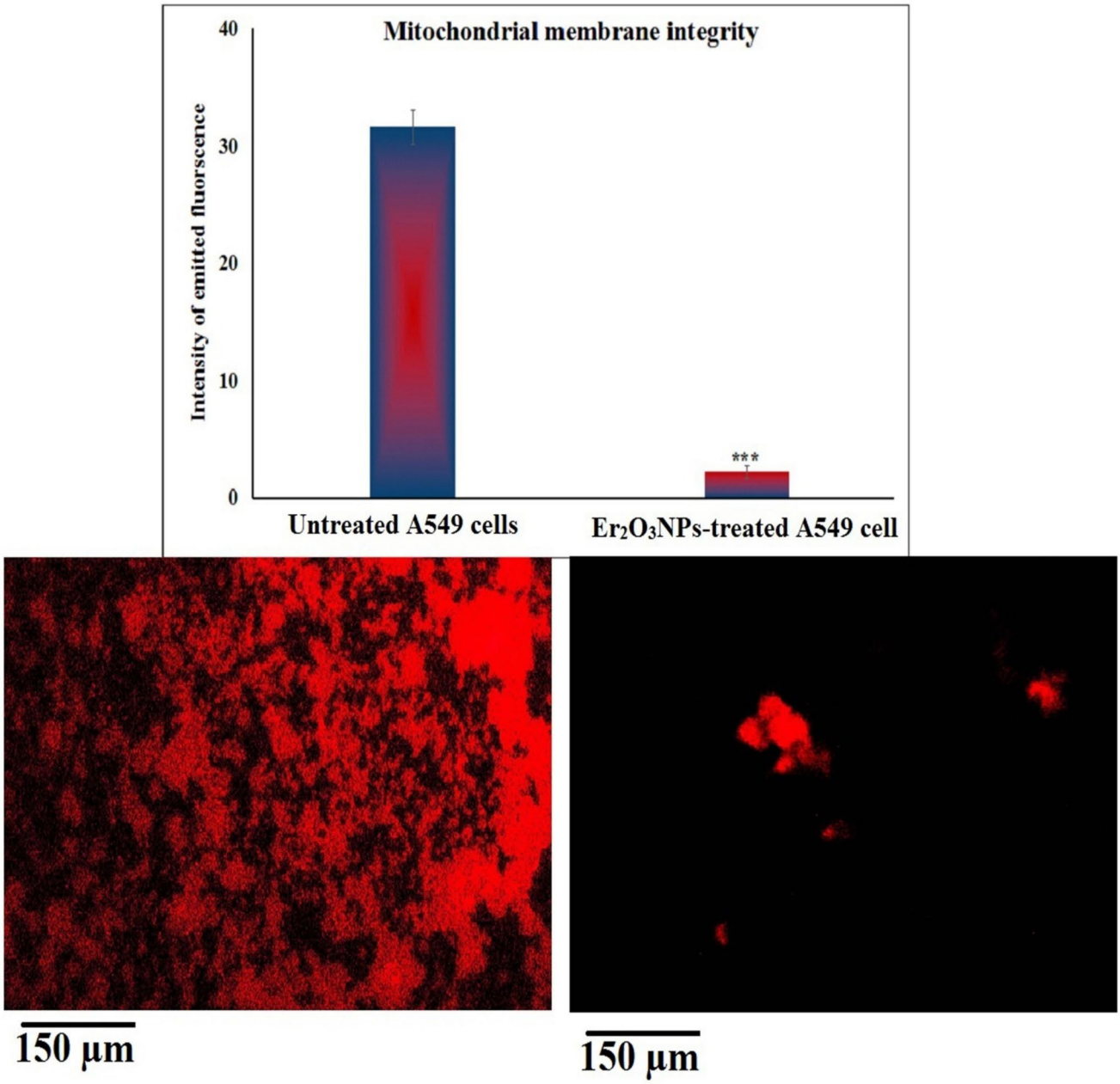

Fig. 4 Qualitative and quantitative analysis of mitochondrial membrane potential integrity using Rhodamine-123 fluorescent probe, in the untreated and treated non-small A549 lung cancer cells with the IC50 concentration (93.46 µg/ml) of Er_2O_3NPs for 72 h. Magnification 200x

features, including nuclear shrinkage, chromatin condensation, fragmentation, and formation of apoptotic bodies, which appeared as brightly stained condensed nuclei under fluorescence microscopy (Fig. 6). Statistical analysis confirmed a significant increase ($p < 0.001$) in the proportion of apoptotic nuclei in Er_2O_3NPs-treated cells relative to untreated control A549 lung cancer cells (Table 4). Collectively, these findings confirm that Er_2O_3NPs induce pronounced apoptosis in A549 lung cancer cells, as evidenced by chromatin fragmentation and nuclear disintegration. The results highlight the strong pro-apoptotic potential of Er_2O_3NPs and their promise as a nanotherapeutic candidate for targeted treatment of NSCLC.

Er_2O_3NPs cause significant downregulation of p53, ND3 and Bcl2 gene expression in A549 lung cancer cells

Results of qRT-PCR analysis displayed that treatment of non-small A549 lung cancer cells with Er_2O_3NPs at the

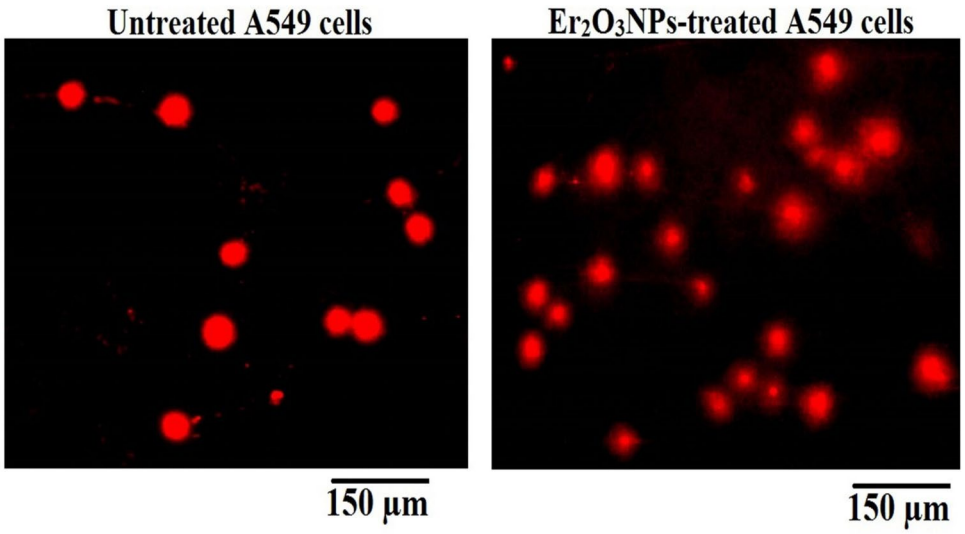

Fig. 5 Fluorescence microscopy of chromatin-diffused cells shows that untreated A549 control cells maintain intact nuclear DNA, whereas A549 cells treated with Er_2O_3NPs at the IC50 concentration (93.46 µg/ml) for 72 h exhibit pronounced DNA diffusion, characteristic of apoptosis. Magnification: 200×

Table 3 Incidence of apoptosis induction in human non-small A549 lung cancer cells detected by chromatin diffusion assay following exposure to the IC50 concentration (93.46 µg/ml) of Er_2O_3NPs for 72 h

Cells	Treatment (Concentration)	Number of cells with		Percentage of apoptotic cells
		intact DNA	diffused DNA	
A549 lung cancer cells	Untreated (0.00 µg/ml)	920.00 ± 5.57	80.00 ± 5.57	8.00 ± 0.56
	Er_2O_3NPs-treated (93.46 µg/ml)	503.33 ± 20.82***	496.67 ± 20.82***	49.67 ± 2.08***

Results are expressed as mean ± SD

***: Indicates statistical significant difference from the compared untreated control cells at $p < 0.001$, using *independent student t-test*

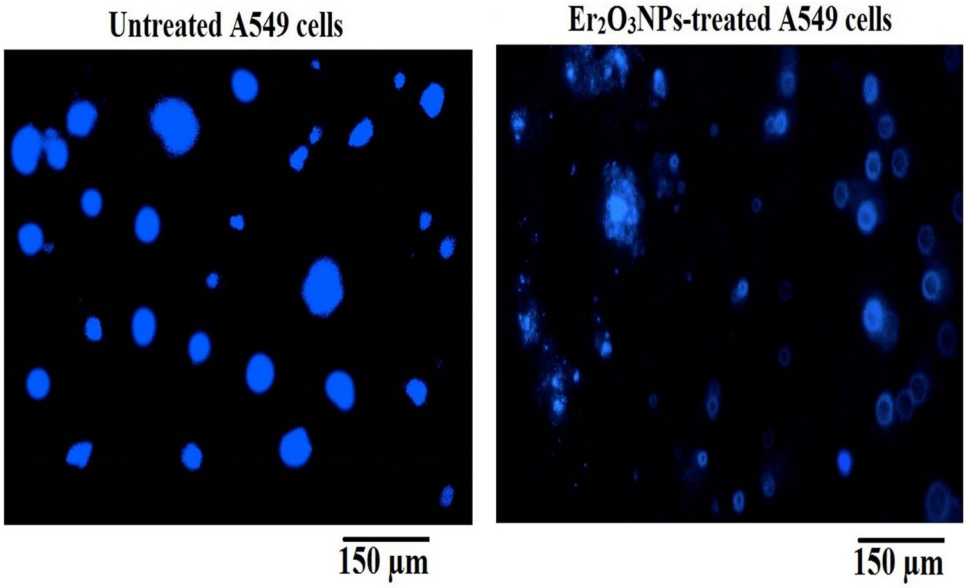

Fig. 6 Fluorescence microscopy of DAPI-stained A549 cells shows intact, uniformly stained nuclei in untreated control cells, while A549 cells treated with Er_2O_3NPs at the IC50 concentration (93.46 µg/mL) for 72 h display condensed and fragmented nuclei, indicative of apoptosis. Magnification: 200×

IC_{50} concentration (93.46 µg/ml) for 72 h caused a profound alteration ($p < 0.001$) in the transcriptional expression level of genes associated with apoptosis regulation and mitochondrial function as seen in Table 5. Notably, the expression level of *p53, ND3,* and *Bcl-2* were all significantly downregulated ($p < 0.001$) in Er_2O_3NPs-treated A549 lung cancer cells compared to untreated control A549 cells. The pronounced suppression of the *p53* gene, a central regulator of DNA

Table 4 Incidence of apoptosis induction in human non-small A549 lung cancer cells detected by DAPI staining assay following exposure to the IC50 concentration (93.46 µg/ml) of Er_2O_3NPs for 72 h

Cells	Treatment (Concentration)	Number of cells with		Percentage of apoptotic cells
		intact DNA	fragmented and condensed DNA	
A549 lung cancer cells	Untreated (0.00 µg/ml)	935.00 ± 4.00	65.00 ± 4.00	6.50 ± 0.40
	Er_2O_3NPs-treated (93.46 µg/ml)	344.67 ± 17.67***	655.33 ± 17.67 ***	65.53 ± 1.77 ***

Results are expressed as mean ± SD

***: Indicates statistical significant difference from the compared untreated control cells at $p < 0.001$, using *independent student t-test*

Table 5 Expression level of pro-apoptotic *p53,* mitochondrial *ND3* and anti-apoptotic *Bcl2* genes in in human non-small A549 lung cancer cells following exposure to the IC50 concentration (93.46 µg/ml) of Er_2O_3NPs for 72 h

Cells	Treatment (Concentration)	Fold change in expression level of		
		p53	*ND3*	*Bcl2*
A549 lung cancer cells	Untreated (0.00 µg/ml)	1.00 ± 0.00	1.00 ± 0.00	1.00 ± 0.00
	Er_2O_3NPs-treated (93.46 µg/ml)	0.06 ± 0.01***	0.48 ± 0.03 ***	0.27 ± 0.01 ***

Results are expressed as mean ± SD

***: Indicates statistical significant difference from the compared untreated control cells at $p < 0.001$, using *independent student t-test*

damage response and apoptosis, suggests that Er_2O_3NPs-induced cell death occurs predominantly through a *p53*-independent apoptotic pathway.

Concurrently, the significant decrease in *ND3* gene expression, a key subunit of mitochondrial complex I, indicates severe mitochondrial dysfunction and disruption of oxidative phosphorylation, potentially leading to excessive ROS generation and mitochondrial membrane depolarization. Similarly, the observed marked downregulation of the anti-apoptotic *Bcl-2* gene reflects a loss of mitochondrial membrane integrity and diminished cellular defense against oxidative and apoptotic stimuli. This reduction in *Bcl-2* expression likely exacerbates mitochondrial outer membrane permeabilization, facilitating cytochrome c release and activation of downstream apoptotic cascades. Collectively, these findings demonstrate that Er_2O_3NPs exert their cytotoxic effects on A549 lung cancer cells by simultaneously suppressing *p53, ND3*, and *Bcl-2* gene expression, thereby promoting mitochondrial dysfunction, loss of cellular bioenergetics, and activation of intrinsic apoptosis. This coordinated gene downregulation highlights the potential of Er_2O_3NPs as a promising nanotherapeutic candidate capable of targeting mitochondrial integrity and apoptotic regulation in non-small cell lung cancer.

Discussion

Overcoming the severe systemic toxicity and poor tumor selectivity of conventional chemotherapy demands the urgent development of novel, targeted nanotherapeutics. Despite rare-earth metal oxides possess highly promising physicochemical properties, their therapeutic potential and organelle-level apoptotic mechanisms in lung malignancies have remained largely unexplored. To address these critical challenges, the present study investigated the antitumor potential of Er_2O_3NPs in an in vitro NSCLC model and successfully demonstrated their preferential cytotoxic activity against lung cancer cells. Specifically, MTT assay findings reveal that Er_2O_3NPs exert concentration-dependent cytotoxicity against cancerous A549 cells while displaying lower toxicity toward normal WI-38 fibroblasts, yielding a moderate selectivity index of 1.58. This preferential targeting aligns with previous studies demonstrating that rare-earth and metal oxide nanoparticles selectively target cancer cells because of their altered oxidative metabolism, elevated oxidative stress, and distinct membrane potential (Jeon et al. 2025; Mohamed et al. 2023; Yassin et al. 2024; Mohamed et al. 2025a; Titova et al. 2025). By exploiting these cancer-unique vulnerabilities, Er_2O_3NPs offer a promising therapeutic alternative that could minimize the collateral damage to normal tissues while maintaining potent antitumor efficacy, thereby addressing a critical limitation of conventional chemotherapy. Collectively, these findings highlight Er_2O_3NPs as promising candidates for selective lung cancer therapy and provide a strong foundation for subsequent mechanistic investigations, as well as future biodistribution and *in vivo* safety studies.

Crucially, our mechanistic investigations revealed that the preferential cytotoxicity of Er_2O_3NPs toward A549 cells is driven by a coordinated, complex, multi-step apoptotic

cascade initiated by excessive intracellular ROS generation. As schematically illustrated in Fig. 7, this pronounced overproduction of ROS disrupts cellular redox homeostasis, causing extensive oxidative damage to lipids, proteins, and DNA, which ultimately triggers severe genomic instability. This oxidative stress is accompanied by pronounced mitochondrial dysfunction, evidenced by mitochondrial membrane depolarization, indicating impairment of mitochondrial integrity and activation of the intrinsic apoptotic pathway. These organelle-level alterations are further validated by the classical morphological hallmarks of apoptosis, including chromatin condensation, nuclear fragmentation, and apoptotic body formation observed following nuclear staining of Er_2O_3NPs-treated A549 cells. Concurrently, Er_2O_3NPs exposure significantly altered the expression of key genes involved in mitochondrial function and cell survival, as demonstrated by the marked downregulation of *p53*, *ND3*, and *Bcl-2* transcripts. Specifically, the suppression of *ND3* (a critical subunit of mitochondrial Complex I) likely intensifies respiratory chain impairment and ROS production, whereas the depletion of the anti-apoptotic guardian *Bcl-2* destabilizes the outer mitochondrial membrane amplifying downstream apoptotic signaling. Collectively, by integrating these precise cellular, organellar, and transcriptional findings, this study provides the first comprehensive evidence that Er_2O_3NPs induce a ROS-driven intrinsic mitochondrial apoptotic cascade

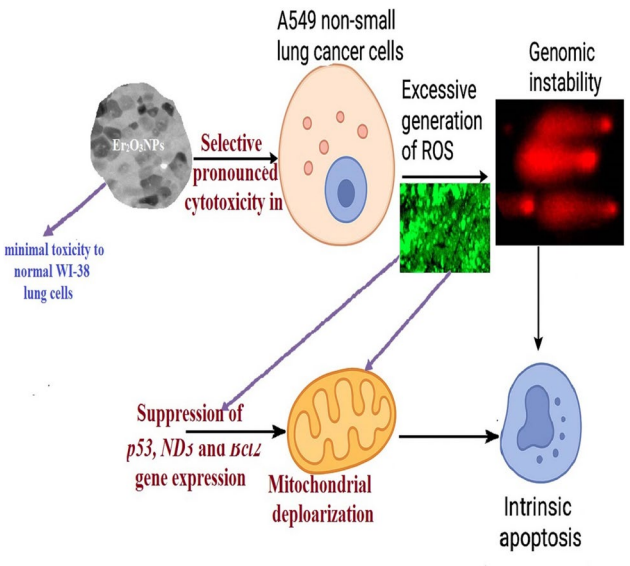

Fig. 7 Schematic summary of the proposed mechanism of Er_2O_3NPs-induced cytotoxicity in A549 human non-small cell lung cancer cells based on the experimental findings of the present study. The diagram illustrates the observed ROS overproduction, genomic DNA damage, mitochondrial membrane depolarization, downregulation of *p53*, *ND3*, and *Bcl-2* mRNA expression, and the resulting mitochondrial apoptotic response

in lung cancer cells, shifting the experimental paradigm from broad cytotoxic screening to targeted, organelle-specific dysfunction and highlighting organelle-specific mitochondrial dysfunction as a central driver of Er_2O_3NPs selective anticancer activity. The individual findings and their biological significance are discussed in detail in the following points.

The results of the alkaline comet assay confirmed substantial DNA strand breaks and extensive genomic instability in Er_2O_3NPs-treated A549 lung cancer cells cells, as demonstrated by significant increases in key DNA damage parameters; tail length, %DNA in tail, and tail moment, compared to their values in untreated control A549 cells. These findings are consistent with previous studies demonstrating that Er_2O_3NPs-induced ROS generation causes oxidative DNA damage and strand breaks in human HepG2 hepatocellular carcinoma and U937 lymphoma cells (Safwat et al. 2022; Mohamed et al. 2025). Cancer cells, which already experience chronic oxidative stress and reduced antioxidant capacity, are particularly vulnerable to such additional ROS-induced genotoxic insults (Valko et al. 2006; Tomasetti et al. 2015). Over ROS production was manifested in this study through the marked increases in the fluorescence intensity emitted from in Er_2O_3NPs-treated A549 cancer cells compared to untreated A549 cells. Therefore, the extensive DNA damage observed in this study can be attributed to ROS overproduction triggered by Er_2O_3NPs exposure, establishing a direct mechanistic link between oxidative stress, genomic instability, and apoptotic cell death in A549 lung cancer cells.

Mitochondrial dysfunction emerged as a pivotal event in the cytotoxic mechanism induced by Er_2O_3NPs in A549 lung cancer cells (Mohamed et al. 2025). Rhodamine-123 staining revealed a marked and statistically significant reduction in mitochondrial membrane potential following exposure to Er_2O_3NPs, indicating profound mitochondrial depolarization and structural destabilization of the inner mitochondrial membrane in Er_2O_3NPs-treated A549 cells. The dissipation of mitochondrial membrane potential represents one of the earliest and most critical biochemical hallmarks of intrinsic (mitochondrial-mediated) apoptosis, as it signifies the loss of mitochondrial integrity and initiates the release of cytochrome c and other pro-apoptotic factors from the intermembrane space into the cytosol. This release subsequently triggers the activation of caspase-9 and caspase-3, orchestrating the execution phase of apoptosis (Gupta et al. 2009; Chu et al. 2021).

The observed mitochondrial collapse is likely driven by Er_2O_3NPs-induced oxidative stress, as excessive ROS generation can directly damage mitochondrial lipids, proteins, and respiratory chain complexes, impairing electron transport and ATP synthesis. Damage to complex I, where the ND3 subunit resides, may further amplify

electron leakage and superoxide formation, perpetuating a self-reinforcing cycle of oxidative stress and mitochondrial injury. Similar patterns of ROS-mediated mitochondrial depolarization have been reported in Er_2O_3NPs- treated U937 lymphoma cells and other cells exposed to other metal oxide nanoparticles, confirming this as a conserved mechanism of nanoparticle-induced apoptosis (Mohamed et al. 2025; Mohamed et al. 2025a; Mohamed et al. 2025b; Mohamed et al. 2025c). Given that cancer cells are highly dependent on mitochondrial bioenergetics and redox signaling to sustain rapid proliferation and survival under oxidative stress, disruption of mitochondrial function by Er_2O_3NPs may render them particularly vulnerable to apoptosis. In contrast, normal WI fibroblasts, which possess stronger antioxidant defenses and greater metabolic adaptability, appear to withstand similar exposure levels, reflecting the selective toxicity of Er_2O_3NPs. Thus, mitochondrial depolarization constitutes a central and selective mechanism by which Er_2O_3NPs compromise cancer cell viability, linking oxidative damage to bioenergetic collapse and apoptotic cell death in non-small cell lung cancer.

Nuclear and molecular analyses provided compelling evidence confirming that Er_2O_3NPs induce apoptosis in A549 lung cancer cells through an intrinsic, mitochondria-dependent mechanism. Nuclear staining assays, including both chromatin diffusion and DAPI fluorescence microscopy, revealed characteristic apoptotic nuclear changes in Er_2O_3NPs-treated A549 cells compared with untreated control A549 lung cancer cells. Morphological examination demonstrated pronounced chromatin condensation, nuclear shrinkage, and extensive fragmentation, along with the formation of apoptotic bodies, hallmark features of programmed cell death (Elmore 2007; Guo et al. 2025). In contrast, nuclei of untreated control A549 cells remained smooth, round, and uniformly stained, indicating normal nuclear integrity. The distinct chromatin dispersion patterns visualized in the chromatin diffusion assay further confirmed DNA fragmentation and endonuclease activation, both of which occur during late-stage apoptosis. These nuclear alterations strongly correlate with Er_2O_3NPs-induced oxidative stress and mitochondrial dysfunction, supporting the hypothesis that Er_2O_3NPs trigger apoptosis through a ROS-dependent mitochondrial signaling cascade.

Molecular analysis provided deeper mechanistic insights into the intracellular cascades triggered by Er_2O_3NPs exposure in human NSCLC cells. In this study, treatment with Er_2O_3NPs at the IC50 concentration (93.46 µg/ml) for 72 h significantly downregulated the mRNA expression of *p53*, *ND3*, and *Bcl-2* gene expression compared to untreated control A549 cells. To accurately interpret the observed reduction in *p53* transcripts, it is essential to consider the specific genetic background of the A549 cell line. These A549 cells inherently harbor a heterozygous point mutation in the TP53 gene (G288V) within the DNA-binding domain, which is associated with impaired canonical *p53* transcriptional activity and altered apoptotic signaling (Klimovich et al. 2021; Zhang et al. 2025). Accordingly, the decrease in *p53* mRNA expression level observed following Er_2O_3NPs treatment is compatible with the compromised *p53* signaling characteristic of this genetically mutant cell line. However, these transcriptional findings alone are insufficient to conclude that the apoptotic response occurs entirely independently of *p53* function. This consideration is crucial because *p53* is a multifunctional regulator of cell death that mediates apoptosis through both transcription-dependent and transcription-independent pathways (Mohamed et al. 2025b; Mohamed et al. 2025; Hao et al. 2023).

Notably, the tumor suppressor *p53* beyond its classic well-established role as a nuclear transcription factor, can also directly promote mitochondrial apoptosis through a transcription-independent mechanism under severe oxidative and genotoxic stress. Under such cellular stress conditions, even mutant *p53* protein can escape degradation, undergo rapid stabilization and post-translational modifications; most notably phosphorylation and acetylation. Once modified, *p53* translocates to the outer mitochondrial membrane, where it activates the pro-apoptotic proteins *BAX* and *BAK* and antagonizes the anti-apoptotic proteins *Bcl-2* and *Bcl-xL*, thereby disrupting mitochondrial membrane integrity and activating the intrinsic apoptotic cascade (Mohamed et al. 2025; Hao et al. 2023). Because these cytoplasmic mitochondrial functions occur independently of gene transcription, they cannot be inferred from *p53* mRNA expression alone. Consequently, despite Er_2O_3NPs treatment markedly reduced *p53* mRNA expression in A549 cells after 72 h, this finding alone is insufficient to conclude that Er_2O_3NPs-induced apoptosis in A549 cells occurs entirely independently of *p53*. Nevertheless, the findings of excessive ROS generation, severe genomic DNA damage, mitochondrial membrane depolarization, and extensive nuclear fragmentation demonstrated in Er_2O_3NPs-exposed A549 cells provide strong evidence for activation of the intrinsic mitochondrial apoptotic pathway (Mohamed et al. 2025b; Mohamed et al. 2025). These observations are consistent with previous studies showing that nanoparticle-induced apoptosis is predominantly mediated by oxidative stress and mitochondrial dysfunction, even in cellular models with impaired canonical *p53* signaling (Mohamed et al. 2025b; Mohamed et al. 2025; Hao et al. 2023). Therefore, our results support ROS-driven mitochondrial dysfunction as the principal mechanism underlying Er_2O_3NPs-induced apoptosis, accompanied by reduced *p53* mRNA expression, rather than demonstrating a definitive *p53*-independent apoptotic pathway.

Concomitantly, the significant transcriptional downregulation of *ND3*, a core subunit of mitochondrial complex I, disrupted mitochondrial oxidative phosphorylation and diminished ATP synthesis, thereby results in electron leakage and excessive ROS accumulation. This increase in ROS generation further exacerbates oxidative stress and mitochondrial membrane damage, establishing a self-reinforcing feed-forward loop of redox imbalance and apoptosis. In parallel, the marked downregulation of the anti-apoptotic *Bcl-2* gene expression compromises mitochondrial membrane integrity, weakening the cell's defense against pro-apoptotic signals. This decline in *Bcl-2* expression facilitates mitochondrial outer membrane permeabilization, enabling the cytosolic release of cytochrome *c* and the subsequent activation of caspase-dependent intrinsic apoptotic cascades (Suhaili et al. 2017; Vogler et al. 2025). Collectively, these morphological and molecular findings confirm that Er_2O_3NPs induce apoptosis in A549 lung cancer cells through a mitochondrial-mediated, p53-independent pathway. The coordinated nuclear fragmentation, mitochondrial depolarization, and transcriptional suppression of *p53*, *ND3*, and *Bcl-2* highlight a multifaceted mechanism in which oxidative stress and mitochondrial dysfunction converge to drive intrinsic apoptosis. These results provide strong mechanistic evidence of the anticancer potential of Er_2O_3NPs; underscoring their promise as redox-active nano-therapeutic agents for NSCLC.

Based on the above findings, Er_2O_3NPs-induced apoptosis in A549 cells proceeds predominantly through a *p53*-independent mitochondrial pathway, providing a crucial mechanistic distinction from classical apoptosis inducers. Unlike conventional mitochondrial toxins, such as rotenone or antimycin A, which directly inhibit specific electron transport chain complexes and often cause broad cytotoxicity in both normal and malignant cells (Wang et al. 2009; Gu et al. 2016), Er_2O_3NPs initiate mitochondrial dysfunction indirectly by promoting ROS overproduction, inducing genomic instability, and suppressing critical mitochondrial survival genes including *ND3* and *Bcl2*. This multifaceted mechanism enables selective cytotoxicity toward cancer cells, as demonstrated by the relatively lower sensitivity of WI-38 fibroblasts observed in this study. Furthermore, Er_2O_3NPs-mediated mitochondrial impairment integrates oxidative stress with transcriptional modulation, potentially overcoming resistance mechanisms associated with conventional mitochondrial toxins and providing an alternative strategy for targeting apoptosis in *p53*-compromised cancer cells. these findings therefore suggest that Er_2O_3NPs-induced mitochondrial apoptosis offers both mechanistic versatility and therapeutic advantages over traditional mitochondrial-targeting approaches. Nevertheless, further in vivo studies are required to comprehensively evaluate its safety, selectivity, and therapeutic efficacy.

This study consequently is the first to comprehensively investigate the selective cytotoxic and mechanistic actions of Er_2O_3NPs against non-small A549 lung cancer cells, demonstrating potent, concentration-dependent cytotoxicity toward A549 lung cancer cells while sparing normal WI lung fibroblasts. The results reveal also that Er_2O_3NPs trigger a cascade of ROS overproduction, mitochondrial depolarization, genomic instability, and coordinated suppression of apoptosis- and Mitochondrial function-related genes. However, the present study has some limitations, including its restriction to in vitro experimentation using a single NSCLC cell line (A549), which cannot fully mimic the physiological complexity of the in vivo tumor microenvironment and may limit the generalizability of the findings. In addition, all mechanistic investigations were performed only at the IC_{50} concentration; therefore, concentration-dependent responses were not evaluated. The study was also limited to transcript-level analyses and did not assess key protein-level apoptotic markers, including cytochrome c release, caspase activation, or *p53* protein expression, post-translational modifications, and mitochondrial translocation. Furthermore, the long-term safety, biodistribution, pharmacokinetics, and systemic toxicity of Er_2O_3NPs under in vivo conditions remain unknown, and their potential synergistic effects with conventional chemotherapeutic agents were not investigated. Future studies should therefore incorporate additional NSCLC cell lines, such as H1299 and H460, perform concentration–response mechanistic analyses, and validate the the antitumor efficacy and systemic safety of Er_2O_3NPs in appropriate in vivo NSCLC models. Furthermore, comprehensive proteomic and metabolic analyses are warranted to further elucidate the molecular mechanisms underlying Er_2O_3NPs-induced cytotoxicity. In particular, protein-level investigations, including Western blot analysis of downstream apoptotic markers, cytochrome c release, caspase activation, and assessment of *p53* protein expression, post-translational modifications, and mitochondrial localization, are needed to define the precise contribution of *p53* to the observed apoptotic response. Finally, evaluating Er_2O_3NPs in combination with established chemotherapeutic agents may identify synergistic therapeutic strategies that enhance antitumor efficacy while minimizing off-target toxicity.

Conclusion

Overall, the current study demonstrates that Er_2O_3NPs exhibit concentration-dependent, preferential cytotoxicity against human A549 lung cancer cells compared to normal WI-38 lung fibroblasts, yielding a moderate selectivity index of 1.58. Mechanistically, our results reveal that Er_2O_3NPs trigger oxidative stress-mediated, mitochondrial-dependent apoptosis.

This cascade is driven primarily by excessive intracellular ROS generation, severe genomic DNA damage, mitochondrial membrane depolarization, and the down-regulation of key apoptosis- and mitochondria-related transcripts (*p53*, *ND3*, and *Bcl-2*). Within the *p53*-mutant genetic context of A549 cells, these molecular and cellular alterations collectively drive programmed cell death by bypassing classical wild-type *p53* transcriptional activation. These findings highlight ROS-mediated intrinsic mitochondrial dysfunction as the primary executionary mechanism of Er_2O_3NPs-induced toxicity, which occurs concurrently with reduced *p53* mRNA expression. Consequently, Er_2O_3NPs hold promise as a potential nanotherapeutic candidate for lung cancer management. Nevertheless, several limitations should be acknowledged. The study was limited to in vitro experiments using a single NSCLC cell line, and all mechanistic analyses were performed only at the IC50 concentration. In addition, only transcript-level changes were assessed, whereas protein-level apoptotic events, including cytochrome c release, caspase activation, and *p53* protein expression, post-translational modifications, and mitochondrial translocation, were not investigated. Furthermore, the long-term safety, biodistribution, pharmacokinetics, and systemic toxicity of Er_2O_3NPs remain unknown, and their potential synergy with conventional chemotherapeutic agents was not evaluated. Future studies should validate these findings in additional NSCLC models and i*n vivo*, incorporate concentration–response and protein-level mechanistic analyses, and investigate combination therapies to further define the therapeutic potential and translational applicability of Er_2O_3NPs for NSCLC management.

Acknowledgements We gratefully acknowledge the Department of Zoology, Faculty of Science, Cairo University, for providing the essential chemicals, materials, and equipment that made this study possible. Their generous support and collaboration were vital to the successful completion of our experiments, and we extend our sincere appreciation for their invaluable contribution to this research.

Authors' contributions Hanan R.H. Mohamed conceived and designed the study, conducted molecular experiments, performed statistical analyses, and drafted the manuscript. Alaa H. Elsewedy, Shahd Mosaad, Habiba M. Zaki, Mayada E. Borai, and Aya A. Osman carried out experimental work and contributed to manuscript writing. Gehan Safwat, Ayman Diab and all authors reviewed and approved the final version of the manuscript. The authors declare that all data were generated in-house and that no paper mill was used.

Funding The current study was partially funded by the Faculty of Science, Cairo University, and the Faculty of Biotechnology at October University for Modern Sciences and Arts (MSA), Egypt.

Data availability The datasets used and/or analyzed during the current study are available from the corresponding author on reasonable request.

Code availability Not applicable.

Declarations

Consent for publication Not applicable.

Consent for participation Not applicable.

Clinical trials Not applicable.

Competing interests The authors declare no competing interests.

References

Abdelsalam EA, Abd El-Hafeez AA, Eldehna WM, El Hassab MA, Marzouk HMM, Elaasser MM, Abou Taleb NA, Amin KM, Abdel-Aziz HA, Ghosh P, Hammad SF (2022) Discovery of novel thiazolyl-pyrazolines as dual EGFR and VEGFR-2 inhibitors endowed with in vitro antitumor activity towards non-small lung cancer. J Enzyme Inhib Med Chem 37(1):2265–2282. https://doi.org/10.1080/14756366.2022.2104841

Bray F, Laversanne M, Sung H, Ferlay J, Siegel RL, Soerjomataram I, Jemal A (2024) Global cancer statistics 2022: GLOBOCAN estimates of incidence and mortality worldwide for 36 cancers in 185 countries. CA Cancer J Clin 74(3):229–263. https://doi.org/10.3322/caac.21834

Chehelgerdi M, Chehelgerdi M, Allela OQB, Pecho RDC, Jayasankar N, Rao DP, Thamaraikani T, Vasanthan M, Viktor P, Lakshmaiya N, Saadh MJ, ..., Akhavan-Sigari R (2023). Progressing nanotechnology to improve targeted cancer treatment: overcoming hurdles in its clinical implementation. Mol Cancer 22(1):169. https://doi.org/10.1186/s12943-023-01865-0

Chu Q, Gu X, Zheng Q, Wang J, Zhu H (2021) Mitochondrial mechanisms of apoptosis and necroptosis in liver diseases. Anal Cell Pathol (Amst) 2021:8900122. https://doi.org/10.1155/2021/8900122

Duma N, Santana-Davila R, Molina JR (2019) Non–small cell lung cancer: Epidemiology, screening, diagnosis, and treatment. Mayo Clin Proc 94(8):1623–1640. https://doi.org/10.1016/j.mayocp.2019.01.013

Elmore S (2007) Apoptosis: a review of programmed cell death. Toxicol Pathol 35(4):495–516. https://doi.org/10.1080/01926230701320337

El-Zahabi HSA, Khalifa MMA, Gado YMH, Farrag AM, Elaasser MM, Safwat NA, AbdelRaouf RR, Arafa RK (2019) New thiobarbituric acid scaffold-based small molecules: synthesis, cytotoxicity, 2D-QSAR, pharmacophore modelling and in-silico ADME screening. Eur J Pharm Sci 130:124–136. https://doi.org/10.1016/j.ejps.2019.01.023

Grzybowska-Szatkowska L, Ślaska B (2014) Mitochondrial NADH dehydrogenase polymorphisms are associated with breast cancer in Poland. J Appl Genet 55:173–181

Gu S, Chen C, Jiang X, Zhang Z (2016) ROS-mediated endoplasmic reticulum stress and mitochondrial dysfunction underlie apoptosis induced by resveratrol and arsenic trioxide in A549 cells. Chem Biol Interact 245:100–109. https://doi.org/10.1016/j.cbi.2016.01.005

Guan X, Guan Y (2020) Artemisinin induces selective and potent anticancer effects in drug resistant breast cancer cells by inducing cellular apoptosis and autophagy and G2/M cell cycle arrest. J BUON 25(3):1330–1336

Guo J, Yang WT, Mai FY, Liang JR, Luo J, Zhou MC, Yu DD, Wang YL, Li CG (2025) Unravelling oncosis: morphological and molecular insights into a unique cell death pathway. Front Immunol 15:1450998. https://doi.org/10.3389/fimmu.2024.1450998

Gupta S, Kass GE, Szegezdi E, Joseph B (2009) The mitochondrial death pathway: a promising therapeutic target in diseases. J Cell Mol Med 13(6):1004–33. https://doi.org/10.1111/j.1582-4934.2009.00697.x

Hao Q, Chen J, Lu H, Zhou X (2023) The ARTS of p53-dependent mitochondrial apoptosis. J Mol Cell Biol 14(10):1074. https://doi.org/10.1093/jmcb/mjac074

Herbst RS, Morgensztern D, Boshoff C (2018) The biology and management of non-small cell lung cancer. Nature 553(7689):446–454. https://doi.org/10.1038/nature25183

Jeon H, Wang S, Song J, Gill H, Cheng H Update (2025) Management of non-small-cell lung cancer. Lung 203(1):53. https://doi.org/10.1007/s00408-025-00801-x

Klimovich B, Merle N, Neumann M, Elmshäuser S, Nist A, Mernberger M, Kazdal D, Stenzinger A, Timofeev O, Stiewe T (2021) p53 partial loss-of-function mutations sensitize to chemotherapy. Oncogene 41(7):1011–1023. https://doi.org/10.1038/s41388-021-02141-5

Lai CY, Tsai AC, Chen MC, Chang LH, Sun HL, Chang YL, Chen CC, Teng CM, Pan SL (2013) Aciculatin induces p53-dependent apoptosis via mdm2 depletion in human cancer cells in vitro and in vivo. PLoS ONE 7(8):e42192

Langie SA, Azqueta A, Collins AR (2015) The comet assay: past, present, and future. Front Genet 6:266

Mehtab A, Ahmed J, Alshehri SM, Mao Y, Ahmad T (2022) Rare earth doped metal oxide nanoparticles for photocatalysis: a perspective. Nanotechnol 33(14). https://doi.org/10.1088/1361-6528/ac43e7

Mohamed HEA, Khalil AT, Hkiri K, Ayaz M, Abbasi JA, Sadiq A, Ullah F, Nawaz A, Ullah I, Maaza M (2023) Physicochemical and nanomedicine applications of phyto-reduced erbium oxide (Er2O3) nanoparticles. AMB Express 13(1):24. https://doi.org/10.1186/s13568-023-01527-w

Mohamed HR, Hemdan SHA, El-Sherif AA (2025a) Y2O3NPs induce selective cytotoxicity, genomic instability, oxidative stress and ROS mediated mitochondrial apoptosis in human epidermoid skin A-431 Cancer cells. Sci Rep 15(1):1543. https://doi.org/10.1038/s41598-024-82376-w

Mohamed HRH, Mohamed BA, Hakeem GM, Elnawasani SH, Nagy M, Essam R, Diab A, Safwat G (2025b) Cobalt oxide nanoparticles induce cytotoxicity and excessive ROS mediated mitochondrial dysfunction and p53-independent apoptosis in melanoma cells. Sci Rep 15:2220. https://doi.org/10.1038/s41598-025-85691-y

Mohamed HRH, Essam R, Mohamed BA, Hakeem GM, Elnawasani SH, Nagy M, Safwat G, Ayman DiabEssam R (2025c) Potent cytotoxicity and induction of ROS-mediated genomic instability, mitochondrial dysfunction, and apoptosis by Y2O3 NPs in Hep-G2 hepatic cancer cells. Naunyn-Schmiedeberg's Arch Pharmacol 398:12673–12683. https://doi.org/10.1007/s00210-025-04051-9

Mohamed HRH, Elberry YA, Magdy H, Ismail M, Michael M, Eltayeb N, Safwat G (2025) Erbium oxide nanoparticles induce potent cell death, genomic instability and ROS-mitochondrial dysfunction-mediated apoptosis in U937 lymphoma cells. Naunyn Schmiedebergs Arch Pharmacol 398(8):11027–11039. https://doi.org/10.1007/s00210-025-03962-x

Mohamed HRH, Michael M, Elberry Y, Magdy H, Ismail M, Eltayeb N, Safwat G, Diab A (2025) Induction of potent preferential cell death, severe DNA damage and p53-independent ROS-mediated mitochondrial apoptosis by CaTiO3NPs in HNO-97 tongue cancer cells. Naunyn Schmiedebergs Arch Pharmacol https://doi.org/10.1007/s00210-025-04323-4

Mosmann T (1983) Rapid colorimetric assay for cellular growth and survival: application to proliferation and cytotoxicity assays. J Immunol Methods 65:55–63

Nasim F, Sabath BF, Eapen GA (2019) Lung cancer. Med Clin North Am 103(3):463–473. https://doi.org/10.1016/j.mcna.2018.12.006

Patra JK, Das G, Fraceto LF, Campos EVR, Rodriguez-Torres MP, Acosta-Torres LS, …, Shin HS (2018) Nano based drug delivery systems: recent developments and future prospects. J Nanobiotechnol 16:71. https://doi.org/10.1186/s12951-018-0392-8

Safwat G, Soliman ESM, Mohamed HRH (2022) Induction of ROS mediated genomic instability, apoptosis and G0/G1 cell cycle arrest by erbium oxide nanoparticles in human hepatic HepG2 cancer cells. Sci Rep 12(1):16333. https://doi.org/10.1038/s41598-022-20830-3

Siddiqui MA, Kashyap MP, Kumar V, Al-Khedhairy AA, Musarrat J et al (2010) Protective potential of trans-resveratrol against 4-hydroxynonenal induced damage in PC12 cells. Toxicol in Vitro 24:1592–1598

Siegel RL, Kratzer TB, Giaquinto AN, Sung H, Jemal A (2025) Cancer statistics, 2025. CA Cancer J Clin 75(1):10–45. https://doi.org/10.3322/caac.21871

Singh NP (2000) A simple method for accurate estimation of apoptotic cells. Exp Cell Res 256(1):328–37. https://doi.org/10.1006/excr.2000.4810

Suhaili SH, Karimian H, Stellato M, Lee TH, Aguilar MI (2017) Mitochondrial outer membrane permeabilization: a focus on the role of mitochondrial membrane structural organization. Biophys Rev 9(4):443–457. https://doi.org/10.1007/s12551-017-0308-0

Sung H, Ferlay J, Siegel RL, Laversanne M, Soerjomataram I, Jemal A, Bray F (2021) Global cancer statistics 2020: GLOBOCAN estimates of incidence and mortality worldwide for 36 cancers in 185 countries. CA Cancer J Clin 71(3):209–249. https://doi.org/10.3322/caac.21660

Suzuki K, Kazui T, Yoshida M, Uno T, Kobayashi T, Kimura T et al (1999) Drug- induced apoptosis and p53, BCL-2 and BAX expression in breast cancer tissues in vivo and in fibroblast cells in vitro. Jpn J Clin Oncol 29(7):323–331

Tice RR, Agurell E, Anerson D, Burlinson B, Hartmann A, Kobayashi H et al (2000) Single cell gel/comet assay: guidelines for in vitro and in vivo genetic toxicology testing. Environ Mol Mutagen 35:206–221

Titova SA, Kruglova MP, Stupin VA, Manturova NE, Silina EV (2025) Potential applications of rare earth metal nanoparticles in biomedicine. Pharmaceuticals (Basel) 18(2):154. https://doi.org/10.3390/ph18020154

Tomasetti M, Santarelli L, Alleva R, Dong LF, Neuzil J (2015) Redox-active and redox-silent compounds: synergistic therapeutics in cancer. Curr Med Chem 22(5):552–68. https://doi.org/10.2174/0929867321666140915142219

Travis WD, Brambilla E, Nicholson AG, Yatabe Y, Austin JH, Beasley MB, …, WHO Panel (2015) The 2015 World Health Organization classification of lung tumors: Impact of genetic, clinical, and radiologic advances since the 2004 classification. J Thoracic Oncol 10(9):1243–1260

Valko M, Rhodes CJ, Moncol J, Izakovic M, Mazur M (2006) Free radicals, metals and antioxidants in oxidative stress-induced cancer. Chem Biol Interact 160(1):1–40. https://doi.org/10.1016/j.cbi.2005.12.009

Vogler M, Braun Y, Smith VM, Westhoff MA, Pereira RS, Pieper NM, Anders M, Callens M, Vervliet T, Abbas M, Macip S, Schmid R, Bultynck G, Dyer MJ (2025) The BCL2 family: from apoptosis mechanisms to new advances in targeted therapy. Signal Transduct Target Ther 10(1):91. https://doi.org/10.1038/s41392-025-02176-0

Wang J, Wang XF, Zhang LG, Xie SY, Li ZL, Li YJ, Li HH, Jiao F (2009) Involvement of the mitochondrial pathway in

p53-independent apoptosis induced by p28GANK knockdown in Hep3B cells. Cytogenet Genome Res. 125(2):87–97. https://doi.org/10.1159/000227831

Yassin MT, Al-Otibi FO, Al-Sahli SA, El-Wetidy MS, Mohamed S (2024) Metal oxide nanoparticles as efficient nanocarriers for targeted cancer therapy: addressing chemotherapy-Induced disabilities. Cancers (Basel) 16(24):4234. https://doi.org/10.3390/cancers16244234

Zhang Y, Jiang L, Jiang L, Geng C, Li L, Shao J, Zhong L (2011) Possible involvement of oxidative stress in potassium bromate-induced genotoxicity in human HepG2 cells. Chem Biol Interact 189(3):186–191

Zhang C, Yang C, Shi Q (2025) Effects of Tp53 gene mutations on the survival of non-small cell lung cancer (NSCLC); a short review. Cancer Manag Res 17:65–82. https://doi.org/10.2147/CMAR.S495006

Zhu Z, Ni J, Cai X, Su S, Zhuang H, Yang Z, Chen M, Ma S, Xie C, Xu Y, Li J, Ge H, Liu A, Zhao L, Rao C, Xie C, Bi N, Hui Z, Zhu G, Yuan Z, ..., Fu X (2022) International consensus on radiotherapy in metastatic non-small cell lung cancer. Transl Lung Cancer Res 11(9):1763–1795. https://doi.org/10.21037/tlcr-22-644